Soft Matter

RSC Publishing

PAPER

Hydrodynamic interactions of self-propelled swimmers

Cite this: *Soft Matter*, 2013, **9**, 4923

John J. Molina,*[a] Yasuya Nakayama[b] and Ryoichi Yamamoto*[a]

The hydrodynamic interactions of a suspension of self-propelled particles are studied using a direct numerical simulation method which simultaneously solves for the host fluid and the swimming particles. A modified version of the "Smoothed Profile" (SP) method is developed to simulate microswimmers as squirmers, which are spherical particles with a specified surface-tangential slip velocity between the particles and the fluid. This simplified swimming model allows one to represent different types of propulsion (pullers and pushers) and is thus ideal to study the hydrodynamic interactions among swimmers. We use the SP method to study the diffusive behavior which arises due to the swimming motion of the particles, and show that there are two basic mechanisms responsible for this phenomena: the hydrodynamic interactions caused by the squirming motion of the particles, and the particle–particle collisions. This dual nature gives rise to two distinct time- and length-scales, and thus to two diffusion coefficients, which we obtain by a suitable analysis of the swimming motion. We show that the collisions between swimmers can be interpreted in terms of binary collisions, in which the effective collision radius is reduced due to the collision dynamics of swimming particles in viscous fluids. At short time-scales, the dynamics of the swimmer is analogous to that of an inert tracer particle in a swimming suspension, in which the diffusive motion is caused by fluid-particle *collisions*. Our results, along with the simulation method we have introduced, will allow us to gain a better understanding of the complex hydrodynamic interactions of self-propelled swimmers.

Received 12th January 2013
Accepted 25th March 2013

DOI: 10.1039/c3sm00140g

www.rsc.org/softmatter

1 Introduction

Swimming microorganisms, from bacteria, to algal cells, to spermatozoa, are ubiquitous in biological processes, and even though the specific propulsion mechanism can vary, the motion of these microswimmers is defined by two basic characteristics: (1) they are moving at very low Reynolds number, where viscous forces are dominant (inertial forces can be neglected), and thus (2) the net force on the body (including the cilia or flagella used to generate the motion) is zero.[1,2] Although we have a clear understanding of how these organisms can generate motion, the physical properties of a suspension of such swimmers are still not completely understood.[3–7] In particular, the rheological properties show a non-trivial dependence on the concentration of swimmers,[8–10] which deviates considerably from that of inert force-free colloidal particles.[11] In addition, hydrodynamic interactions among swimmers have also been shown to give rise to collective motion.[12,13] However, theoretical studies on such phenomena have either neglected the role of hydrodynamic interactions, or used only far-field approximations.[7,14]

In addition to the biological interest of understanding the hydrodynamic interactions of swimming microorganisms, recent experimental work has shown how to design micromotors which can swim in the absence of external fields thanks to interfacial *phoretic* effects,[15–19] which allow the particles to transform the local chemical or thermal energy into mechanical energy. Furthermore, the possibility of using these systems to perform work, whether it be to transport cargo[20,21] or separate particle mixtures,[22] has led to many recent experimental and simulation studies. Although a simple theoretical framework for these swimming systems, which can be used to study the effect of the shape and surface properties on the swimming motion, has already been proposed,[23,24] the collective dynamics, and in particular the role of the hydrodynamic interactions remains an open question. In this paper, we present a direct numerical simulation method (DNS) for self-propelled particles which attempts to overcome this difficulty, by solving the equations of motion for the host fluid as well as the swimming particles.

A detailed description of the swimming mechanism of real microorganisms remains computationally prohibitive, particularly if one is interested in the collective dynamics of such systems; therefore, we must look for a simple generic swimmer, which can be easily modeled, but which manages to reproduce the basic flow properties of actual swimmers, such that the hydrodynamic interactions are accurately reproduced. The "squirmer" model we use was introduced over 50 years ago[25,26] to study the propulsion of spherical ciliate particles, which generate motion through the synchronized beating of an envelope of cilia at their surface. Fortunately, on a mesoscopic

[a]*Department of Chemical Engineering, Kyoto University, Kyoto 615-8510, Japan. E-mail: john@cheme.kyoto-u.ac.jp; ryoichi@cheme.kyoto-u.ac.jp*

[b]*Department of Chemical Engineering, Kyushu University, Fukuoka 819-0395, Japan*

scale, the effect of this surface motion can be replaced by a specified slip velocity between the particle and the fluid. In addition, the parameters of the model can be tuned to mimic different propulsion mechanism, allowing us to study the hydrodynamic interactions of different (idealized) microswimmers within a unified framework. We present a modified "Smoothed Profile" method,[27] previously developed to study colloidal dispersions, which is capable of incorporating this squirming motion by imposing the appropriate slip boundary conditions at the surface of the particles. The advantage of this method is that it allows us to accurately and efficiently include the many-body hydrodynamic interactions among the particles, and it can be easily extended to complex host fluids.

In this work we study the effect of hydrodynamic interactions on the dynamics of a suspension of self-propelled particles. The swimming motion of the particles is known to give rise to a diffusive behavior,[28] even in the absence of thermal fluctuations, and a tracer particle placed in such a system will also undergo diffusion.[29,30] However, the nature of the diffusion is different in both cases, as is evidenced by the different scaling behavior with the concentration of swimmers.[31] In the former case, the diffusion is caused primarily by particle–particle collisions, while the latter is due to the hydrodynamic interactions caused by the squirming motion of the particles. By a suitable analysis of the particle displacements, and the decay in the velocity fluctuations, we show that both phenomena are present in the motion of the squirmers themselves, as should be expected. We are thus able to extract the two underlying time- and length-scales of the system, corresponding to the two distinct diffusive motions, just from the particle trajectories. The importance of this cannot be understated, as these two mechanisms (hydrodynamics and particle collisions) are known to be fundamental in determining the physical properties of swimming suspensions;[32] additionally, measuring tracer diffusion in dense suspensions experimentally can be quite challenging, and the available simulation methods for this are somewhat involved.[31] Finally, using basic results from kinetic theory, we analyze the collisions of the swimmers to derive effective collision radii, which are shown to be independent of concentration, and which depend only on the squirming mode of the swimmers (*i.e.*, the strength of the pusher/puller character). Somewhat surprising is the fact that these effective particle sizes are considerably smaller than the actual size of the particles, which is a consequence of the collision dynamics of swimmers in viscous fluids. This paper is organized as follows: Section 2 introduces the mathematical model of the swimmers and the simulation method, Section 3 validates the computational method against known analytical results, and Section 4 presents the results of our study.

2 The model and methods

2.1 Swimmer model: Blake's squirmers

We consider a simple model of self-propelled spherical swimmers, originally introduced by Lighthill[25] and later extended by Blake,[26] which move due to a self-generated surface-tangential velocity $\boldsymbol{u}^{\mathrm{S}}$. This specific mechanism was proposed as a model for an ideal ciliate particle, in which the synchronized beating of the cilia at the surface gives rise to a net motion, in the absence of any external fields. If one assumes that the displacements of this envelope of cilia are purely tangential, then the effective (time-averaged) slip velocity for these squirmers is given by[26]

$$\boldsymbol{u}^{\mathrm{s}}\left(\hat{\boldsymbol{r}}\right) = \sum_{n=1}^{\infty} \frac{2}{n\left(n+1\right)} B_n \left(\hat{\boldsymbol{e}}\cdot\hat{\boldsymbol{r}}\hat{\boldsymbol{r}} - \hat{\boldsymbol{e}}\right) P_n'\left(\hat{\boldsymbol{e}}\cdot\hat{\boldsymbol{r}}\right) \tag{1}$$

where $\hat{\boldsymbol{e}}$ is the squirmer's fixed swimming axis (*i.e.*, we consider that each squirmer carries with it a fixed coordinate system which determines its preferred swimming direction at each instant), $\hat{\boldsymbol{r}}$ is a unit vector from the particle center to a point on the surface, P_n' is the derivative of the n-th order Legendre polynomial, and B_n is the amplitude of the corresponding mode. Neglecting all squirming modes higher than three, $B_n = 0$ $(n \geq 3)$, the following simple expression for the surface tangential velocity, as a function of the polar angle $\theta = \cos^{-1}(\hat{\boldsymbol{r}}\cdot\hat{\boldsymbol{e}})$, is obtained

$$\boldsymbol{u}^{\mathrm{s}}(\theta) = B_1\left(\sin\theta + \frac{\alpha}{2}\sin 2\theta\right)\hat{\boldsymbol{\theta}} \tag{2}$$

where $\alpha = B_2/B_1$ determines whether the swimmer is a pusher ($\alpha < 0$) or a puller ($\alpha > 0$). An example of the former are spermatozoa and most bacteria, of the latter the unicellular alga *Chlamydomonas*. A schematic representation of the flow profile generated by these two types of swimmers is given in Fig. 1. Although the squirmer model we adopt forgoes describing the detailed propulsion mechanism, it is capable of distinguishing between pushers/pullers and provides an adequate approximation to the far-field flow profile generated by these swimmers. For Newtonian fluids, which is the only case considered here, the swimming speed U of the squirmer is determined uniquely by the first mode B_1, irrespective of the size of the

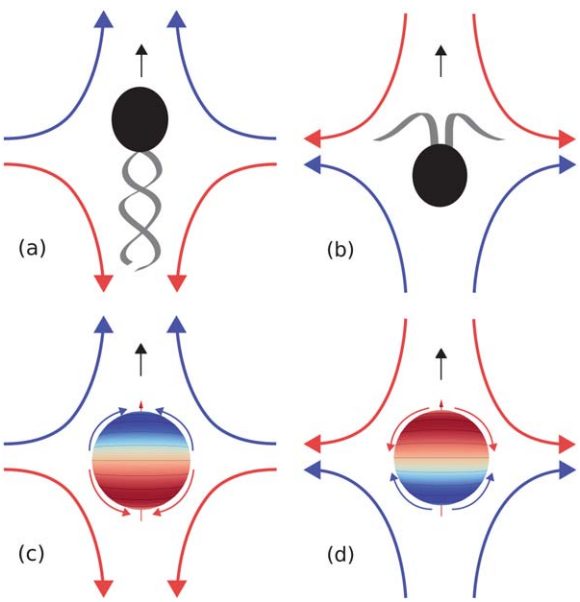

Fig. 1 Schematic representation of the propulsion mechanism and flow profiles of a pusher and a puller, (a) and (b) respectively. These swimmers can be represented using Blake's squirming model, in which the detailed propulsion mechanism is replaced by a specified slip velocity at the surface of the particles, (c) and (d), for pushers and pullers, respectively.

particle, as $U = 2/3B_1$, while the second mode gives the strength of the stresslet.[33,34] The velocity field generated by a single such squirmer, in the Stokes regime, was solved analytically by Ishikawa *et al.*[33] and is given, in the laboratory frame (fluid at rest far away from the particle), by

$$\boldsymbol{u}(\boldsymbol{r}) = B_1 \frac{a^2}{r^2}\left[\frac{a}{r}\left(\frac{2}{3}\hat{\boldsymbol{e}} + \sin\theta\hat{\boldsymbol{\theta}}\right) + \frac{\alpha}{2}\left\{\left(\frac{a^2}{r^2} - 1\right)\left(3\cos^2\theta - 1\right)\hat{\boldsymbol{r}} + \frac{a^2}{r^2}\sin 2\theta\hat{\boldsymbol{\theta}}\right\}\right] \quad (3)$$

where a is the radius of the particle. Notice that for neutral swimmers ($\alpha = 0$) the velocity field decays as r^{-3}, while for pushers/pullers ($\alpha \neq 0$) the velocity field decays as r^{-2}. In contrast, the velocity field for a sedimenting particle (or a particle experiencing a net body force) decays as r^{-1}.[35] This will have important consequences when considering the hydrodynamic interactions of suspensions of swimmers. Finally, although the squirmer model might seem overly simplistic, recent experimental work, focusing on spherical droplets which propel due to self-generated Marangoni stresses at their surface, has shown that it is possible to create such swimmers artificially.[36]

2.2 Simulation method: basic equations

We propose a direct numerical simulation (DNS) procedure to study a system of self-propelled squirmers based on the "Smoothed Profile" (SP) method,[27,37] which allows one to efficiently solve both the Navier–Stokes equation (NS), for the fluid motion, and the Newton–Euler equations, for the colloids. This method has been successfully used to study the diffusion, sedimentation, electro-hydrodynamics, and rheology of colloidal dispersions in incompressible fluids,[38–41] and recent work has shown how it can be extended to treat compressible fluids within a fluctuating-hydrodynamics approach.[42] A detailed error analysis of the method can be found in ref. 43. The basic idea is to replace the sharp boundary at the colloid–fluid interface with a diffuse interface of finite thickness ζ. This allows one to discretize the system using a fixed Cartesian coordinate grid, since the interface will always be supported by multiple-grid points. Although a loss of accuracy at the surface of the particle is inevitable, we can easily impose periodic boundary conditions (PBC), and use a Fourier spectral method to solve for the fluid equations of motion. The particles in the SP method are not treated as boundary conditions for the host fluid, but rather as a body force in the NS equation. Thus, we avoid the mesh-reconstruction problems that plague most computational fluid dynamics methods for systems with moving boundaries. We are aware of two alternative simulation methods that aim to describe these squirmer suspensions at the same level of description, the first was developed by Ramachandran *et al.*[44] using a Lattice Boltzmann (LB) model, and the second was originally introduced by Downton and Stark[45] within a multi-particle collision dynamics (MPC) framework, and later extended by Götze and Gompper[46] to recover the correct rotational dynamics. Although the implementation details are specific to each of the models (LB, MPC, SP), the general mechanism used to obtain the squirming motion is the same in all three cases: local conservation of momentum. For the moment though, these DNS approaches have not been extensively used to study these types of swimming systems; the most popular methods, which still account for the hydrodynamic interactions, have usually been based on Stokesian Dynamics,[8,28,31,33,47–49] and are thus limited to Newtonian fluids in the Stokes regime.

In what follows, we briefly review the governing equations for a dispersion of inert colloids in a simple Newtonian-fluid, before considering how the equations must be modified for use with the SP method for swimming particles with slip boundary conditions. The formulation we present closely follows that of ref. 37, in which a more detailed description of the computational algorithm can be found. The motion of the host fluid is determined by the Navier–Stokes equation with the incompressibility condition

$$\nabla\cdot\boldsymbol{u}_\mathrm{f} = 0 \quad (4)$$

$$\rho(\partial_t + \boldsymbol{u}_\mathrm{f}\cdot\nabla)\boldsymbol{u}_\mathrm{f} = \nabla\cdot\boldsymbol{\sigma} \quad (5)$$

where ρ is the total mass density of the fluid, $\boldsymbol{u}_\mathrm{f}$ is the host fluid velocity field, and $\boldsymbol{\sigma}$ is the stress tensor

$$\boldsymbol{\sigma} = -p\boldsymbol{I} + \boldsymbol{\sigma}' \quad (6)$$

$$\boldsymbol{\sigma}' = \eta[\nabla\boldsymbol{u}_\mathrm{f} + (\nabla\boldsymbol{u}_\mathrm{f})^t] \quad (7)$$

with η the shear viscosity of the fluid. Consider a mono-disperse system of N-spherical particles, of radius a, mass M_p, and moment of inertia $\boldsymbol{I}_\mathrm{p} = 2/5M_\mathrm{p}a^2\boldsymbol{I}$ (with $\boldsymbol{I}$ the unit tensor). The evolution of the colloids is given by the Newton–Euler equations,[50]

$$\begin{aligned} \dot{\boldsymbol{R}}_i &= \boldsymbol{V}_i & \dot{\boldsymbol{Q}}_i &= \mathrm{skew}(\boldsymbol{\Omega}_i)\boldsymbol{Q}_i \\ M_\mathrm{p}\dot{\boldsymbol{V}}_i &= \boldsymbol{F}_i^\mathrm{H} + \boldsymbol{F}_i^\mathrm{C} + \boldsymbol{F}_i^\mathrm{ext} & \boldsymbol{I}_\mathrm{p}\cdot\dot{\boldsymbol{\Omega}}_i &= \boldsymbol{N}_i^\mathrm{H} + \boldsymbol{N}^\mathrm{ext} \end{aligned} \quad (8)$$

where $\boldsymbol{R}_i$ and $\boldsymbol{V}_i$ denote the center of mass position and velocity of particle i, respectively, $\boldsymbol{Q}_i$ is the orientation matrix† and $\boldsymbol{\Omega}_i$ the angular velocity, with skew ($\boldsymbol{\Omega}_i$) the skew-symmetric angular velocity matrix

$$\mathrm{skew}(\boldsymbol{\Omega}_i) = \begin{pmatrix} 0 & -\Omega_i^z & \Omega_i^y \\ \Omega_i^z & 0 & -\Omega_i^x \\ -\Omega_i^y & \Omega_i^x & 0 \end{pmatrix} \quad (9)$$

The forces on the particles are comprised of hydrodynamic contributions arising from the fluid–particle interactions $\boldsymbol{F}^\mathrm{H}$, the colloid–colloid interactions due to the core potential of the particles $\boldsymbol{F}^\mathrm{C}$ (which prevents particle overlap), and a possible external field contribution $\boldsymbol{F}^\mathrm{ext}$ (such as gravity). Likewise, the torques on the particles can be divided into a hydrodynamic $\boldsymbol{N}^\mathrm{H}$ and an external contribution $\boldsymbol{N}^\mathrm{ext}$ (for simplicity, the particle–particle interactions are assumed to be given by a radial potential). In what follows we consider buoyancy-neutral

† For numerical stability we use quaternions, and not rotation matrices, to represent the rigid body dynamics of the particles.

particles, so that $\boldsymbol{F}^{\text{ext}} = \boldsymbol{N}^{\text{ext}} = 0$. Finally, conservation of momentum between the fluid and the particles implies the following hydrodynamic force and torque on the i-th particle

$$\boldsymbol{F}_i^{\text{H}} = \int \mathrm{d}\boldsymbol{S}_i \cdot \boldsymbol{\sigma} \tag{10}$$

$$\boldsymbol{N}_i^{\text{H}} = \int (\boldsymbol{x} - \boldsymbol{R}_i) \times (\mathrm{d}\boldsymbol{S}_i \cdot \boldsymbol{\sigma}) \tag{11}$$

where $\int \mathrm{d}\boldsymbol{S}_i$ indicates an integral over the particle surface.

2.3 Simulation method: smoothed profile squirmers

We now present the computational algorithm used to simulate the motion of spherical particles, with a given surface tangential slip velocity $\boldsymbol{u}^{\text{s}}$, using the SP method. We require that all field variables be defined over the entire computational domain (fluid + particle). The concentration field for the colloids is given as $\phi(\boldsymbol{x},t) = \sum_{i=1}^{N} \phi_i(\boldsymbol{x},t)$, where $\phi_i \in [0, 1]$ is the smooth profile field of particle i. This field is defined such that it is unity within the particle domain, zero in the fluid domain, and smoothly interpolates between both within the interface regions. Details on the specific definition and the properties of this profile function can be found in ref. 27. The particle velocity field is defined in a similar fashion, as

$$\phi \boldsymbol{u}_{\text{p}}(\boldsymbol{x}, t) = \sum_{i=1}^{N} \left\{ \boldsymbol{V}_i(t) + \boldsymbol{\Omega}_i(t) \times \boldsymbol{r}_i(t) \right\} \phi_i(\boldsymbol{x}, t) \tag{12}$$

with $\boldsymbol{r}_i = \boldsymbol{x} - \boldsymbol{R}_i$, which allows one to define the total fluid velocity field as

$$\boldsymbol{u}(\boldsymbol{x},t) \equiv (1 - \phi)\boldsymbol{u}_{\text{f}} + \phi \boldsymbol{u}_{\text{p}} \tag{13}$$

where the incompressibility condition is satisfied on the entire domain $\nabla \cdot \boldsymbol{u} = 0$. The evolution equation for $\boldsymbol{u}$ is then derived assuming momentum-conservation between fluid and particles[27]

$$\rho(\partial_t + \boldsymbol{u} \cdot \nabla)\boldsymbol{u} = \nabla \cdot \boldsymbol{\sigma} + \rho\phi \boldsymbol{f}_{\text{p}} + \rho \boldsymbol{f}_{\text{sq}} \tag{14}$$

where $\phi \boldsymbol{f}_{\text{p}}$ represents the force density field needed to maintain the rigidity constraint on the particle velocity field and $\boldsymbol{f}_{\text{sq}}$ is the force density field generated by the particles' squirming motion.

We use a fractional step approach to update the total velocity field. Let $\boldsymbol{u}^n$ be the field at time $t_n = nh$ (h is the time interval). We first solve for the advection and hydrodynamic viscous stress terms, and propagate the particle positions (orientations) using the current particle velocities. This yields

$$\boldsymbol{u}^* = \boldsymbol{u}^n + \int_{t_n}^{t_n+h} \mathrm{d}s \nabla \cdot \left[\frac{1}{\rho} \left(-p^* \boldsymbol{I} + \boldsymbol{\sigma}' \right) - \boldsymbol{u}\boldsymbol{u} \right] \tag{15}$$

$$\boldsymbol{R}_i^{n+1} = \boldsymbol{R}_i^n + \int_{t_n}^{t_n+h} \mathrm{d}s \boldsymbol{V}_i \tag{16}$$

$$\boldsymbol{Q}_i^{n+1} = \boldsymbol{Q}_i^n + \int_{t_n}^{t_n+h} \mathrm{d}s \,\mathrm{skew}(\boldsymbol{\Omega}_i)\boldsymbol{Q}_i \tag{17}$$

where the pressure term p^* in eqn (15) is determined by the incompressibility condition $\nabla \cdot \boldsymbol{u}^* = 0$. The remaining updating procedure applies to the slip condition at the particle boundary and the rigidity constraint on the velocity field.

We now consider the momentum change needed to maintain the slip velocity at the surface of each of the squirmers, where the slip profile $\boldsymbol{u}^{\text{s}}$ is imposed with respect to the particle velocities $\{\boldsymbol{V}_i';\boldsymbol{\Omega}_i'\}$, using the previously updated positions and orientations $\{\boldsymbol{R}_i^{n+1};\boldsymbol{Q}_i^{n+1}\}$. We note that at this point we do not yet know the updated particle velocities $\{\boldsymbol{V}_i^{n+1};\boldsymbol{\Omega}_i^{n+1}\}$, which are the values that should be used when enforcing the surface slip profile $\boldsymbol{V}_i' = \boldsymbol{V}_i^{n+1}$ ($\boldsymbol{\Omega}_i' = \boldsymbol{\Omega}_i^{n+1}$). Therefore, we adopt an iterative solution, and as an initial guess, we use the particle velocities at the previous time step, *i.e.*, $\boldsymbol{V}_i' = \boldsymbol{V}_i^n$ ($\boldsymbol{\Omega}_i' = \boldsymbol{\Omega}_i^n$). The updated total velocity field is now

$$\boldsymbol{u}^{**} = \boldsymbol{u}^* + \left[\int_{t_n}^{t_n+h} \mathrm{d}s \boldsymbol{f}_{\text{sq}} \right] \tag{18}$$

$$\left[\int_{t_n}^{t_n+h} \mathrm{d}s \boldsymbol{f}_{\text{sq}} \right] = \sum_{i=1}^{N} \varphi_i \left(\boldsymbol{V}_i' + \boldsymbol{\Omega}_i' \times \boldsymbol{r}_i + \boldsymbol{u}_i^{\text{s}} - \boldsymbol{u}^* \right) + \sum_{i=1}^{N} \phi_i (\delta \boldsymbol{V}_i + \delta \boldsymbol{\Omega}_i \times \boldsymbol{r}_i) - \frac{h}{\rho} \nabla p_{\text{sq}} \tag{19}$$

The second term on the right hand side of eqn (19) imposes the slip velocity profile $\boldsymbol{u}^{\text{s}}$ at the surface of each of the squirmers; where $\varphi_i \propto (1 - \phi_i)|\nabla \phi_i|$ is a smooth surface profile function which is non-zero only within the interface domain of the squirmer (normalized such that $|\nabla \phi_i|$ has a maximum value of one), and zero everywhere else. The third term adds a counter-flow entirely within the particle domain, in such a way that local momentum conservation is obtained. Assuming rigid-body motion, with velocities $\delta \boldsymbol{V}_i$ and $\delta \boldsymbol{\Omega}_i$, this requires

$$\int \mathrm{d}\boldsymbol{x} \phi_i (\delta \boldsymbol{V}_i + \delta \boldsymbol{\Omega}_i \times \boldsymbol{r}_i) = -\int \mathrm{d}\boldsymbol{x} \varphi_i (\boldsymbol{V}_i' + \boldsymbol{\Omega}_i' \times \boldsymbol{r}_i + \boldsymbol{u}_i^{\text{s}} - \boldsymbol{u}^*) \tag{20}$$

$$\int \mathrm{d}\boldsymbol{x} \boldsymbol{r}_i \times \phi_i (\delta \boldsymbol{V}_i + \delta \boldsymbol{\Omega}_i \times \boldsymbol{r}_i) = -\int \mathrm{d}\boldsymbol{x} \boldsymbol{r}_i \times \varphi_i (\boldsymbol{V}_i' + \boldsymbol{\Omega}_i' \times \boldsymbol{r}_i + \boldsymbol{u}_i^{\text{s}} - \boldsymbol{u}^*) \tag{21}$$

from which we can easily obtain the counter-flow terms $\delta \boldsymbol{V}_i$ ($\delta \boldsymbol{\Omega}_i$) from the particle velocities $\boldsymbol{V}_i'$ ($\boldsymbol{\Omega}_i'$). A schematic representation of this procedure, used to enforce the specific slip-boundary conditions for our model squirmers, is shown in Fig. 2. Finally, the pressure term due to the squirming motion p_{sq} is obtained from the incompressibility condition $\nabla \cdot \boldsymbol{u}^{**} = 0$. At this point, the momentum conservation is solved for the total velocity field.

The hydrodynamic force and torque exerted by the fluid on the colloids (which includes all contributions due to the squirming motion) is again derived by assuming momentum conservation. The time integrated hydrodynamic force and torque over a period h are equal to the momentum exchange over the particle domain

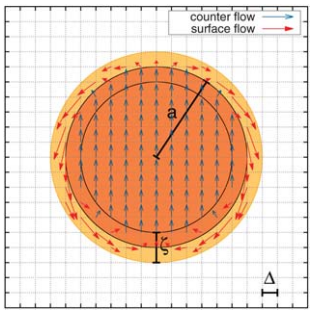

Fig. 2 Schematic representation of the updating scheme used to enforce the slip boundary condition at the surface of the squirmers. Each particle is considered to exert a force on the fluid at the surface, in order to maintain the specified flow profile $\boldsymbol{u}^s$ (red arrows) for the squirming motion. To ensure local momentum conservation, a counter-flow is added within the particle domain (blue arrows).

$$\left[\int_{t_n}^{t_n+h} \mathrm{d}s\left(\boldsymbol{F}_i^{\mathrm{H}}+\boldsymbol{F}_i^{\mathrm{sq}}\right)\right]=\int \mathrm{d}\boldsymbol{x}\,\rho\phi_i^{n+1}\left(\boldsymbol{u}^{**}-\boldsymbol{u}_{\mathrm{p}}^{n}\right) \tag{22}$$

$$\left[\int_{t_n}^{t_n+h} \mathrm{d}s\left(\boldsymbol{N}_i^{\mathrm{H}}+\boldsymbol{N}_i^{\mathrm{sq}}\right)\right]=\int \mathrm{d}\boldsymbol{x}\left[\boldsymbol{r}_i^{n+1}\times\rho\phi_i^{n+1}\left(\boldsymbol{u}^{**}-\boldsymbol{u}_{\mathrm{p}}^{n}\right)\right] \tag{23}$$

From this and any other forces on the colloids, the particle velocities are updated as

$$\boldsymbol{V}_i^{n+1}=\boldsymbol{V}_i^{n}+M_{\mathrm{p}}{}^{-1}\left[\int_{t_n}^{t_n+h}\mathrm{d}s\left(\boldsymbol{F}_i^{\mathrm{H}}+\boldsymbol{F}_i^{\mathrm{sq}}\right)\right]+M_{\mathrm{p}}{}^{-1}\left[\int_{t_n}^{t_n+h}\mathrm{d}s\left(\boldsymbol{F}_i^{\mathrm{C}}+\boldsymbol{F}_i^{\mathrm{ext}}\right)\right] \tag{24}$$

$$\boldsymbol{\Omega}_i^{n+1}=\boldsymbol{\Omega}_i^{n}+\boldsymbol{I}_{\mathrm{p}}{}^{-1}\cdot\left[\int_{t_n}^{t_n+h}\mathrm{d}s\left(\boldsymbol{N}_i^{\mathrm{H}}+\boldsymbol{N}_i^{\mathrm{sq}}\right)\right]+\boldsymbol{I}_{\mathrm{p}}{}^{-1}\cdot\left[\int_{t_n}^{t_n+h}\mathrm{d}s\,\boldsymbol{N}_i^{\mathrm{ext}}\right] \tag{25}$$

We recall that we have imposed the slip profile $\boldsymbol{u}^s$ with respect to the primed velocities $\{\boldsymbol{V}_i';\boldsymbol{\Omega}_i'\}$, which need not be equal to the final velocities of the particle at step $n+1$. To maintain consistency, we iterate over eqn (18)–(25) until convergence in the velocities is achieved. Finally, the resulting particle velocity field $\phi^{n+1}\boldsymbol{u}_{\mathrm{p}}^{n+1}$ is enforced on the total velocity field as

$$\boldsymbol{u}^{n+1}=\boldsymbol{u}^{**}+\left[\int_{t_n}^{t_n+h}\mathrm{d}s\phi\boldsymbol{f}_{\mathrm{p}}\right] \tag{26}$$

$$\left[\int_{t_n}^{t_n+h}\mathrm{d}s\phi\boldsymbol{f}_{\mathrm{p}}\right]=\phi^{n+1}\left(\boldsymbol{u}_{\mathrm{p}}^{n+1}-\boldsymbol{u}^{**}\right)-\frac{h}{\rho}\nabla p_{\mathrm{p}} \tag{27}$$

with the pressure due to the rigidity constraint obtained from the incompressibility condition $\nabla\cdot\boldsymbol{u}^{n+1}=0$. The total pressure field is then given by $p=p^*+p_{\mathrm{p}}+p_{\mathrm{sq}}$.

2.4 Choosing the relevant reference frame

Although we have not included thermal fluctuations in our system, the swimming motion of the particles is known to give rise to diffusive behavior at sufficiently high particle concentrations.[28] However, due to the self-propelled nature of the particles, the largest contribution to their displacement will naturally come from the their inherent swimming. As such, one must wait a very long time before the particles exhibit any type of diffusive behavior, and even then, it is difficult to establish what role the hydrodynamic interactions among neighboring particles are playing. All particles will be swimming in the flow field generated by their neighbors, and the interactions among them can give rise to motion perpendicular to the particle's preferred swimming direction, as well as provide a momentary impulse that can increase/decrease the velocity parallel to the swimming axis, or even change its orientation in space. In order to better understand this phenomena, we analyze the particle motion with respect to the frame of reference of the moving squirmers, as was proposed by Han *et al.*[51] to study the Brownian motion of ellipsoidal particles. We begin by decomposing the particle trajectories in terms of displacements between successive time intervals, which we take to be equally spaced. If $\boldsymbol{R}(t_n)$ denotes the position of a tagged particle at time step n ($t_n=n\delta t$, with δt a suitably small time interval), we can express the time evolution of its position $\{\boldsymbol{R}(t_i)\}$ as

$$\left\{\boldsymbol{R}(t_0),\boldsymbol{R}(t_0)+\Delta_1,\ldots,\boldsymbol{R}(t_0)+\sum_{j=1}^{i}\Delta_j,\ldots,\boldsymbol{R}(t_0)+\sum_{j=1}^{n}\Delta_n\right\} \tag{28}$$

where $\Delta_i=\boldsymbol{R}(t_i)-\boldsymbol{R}(t_{i-1})$. Using this notation, the translational diffusivity is given as[52]

$$D_{\mathrm{T}}(t_n)=\frac{1}{6n\delta t}\left\langle\left(\boldsymbol{R}(t_n)-\boldsymbol{R}(t_0)\right)^2\right\rangle=\frac{1}{6n\delta t}\left\langle\left[\sum_{i=1}^{n}\Delta_n\right]^2\right\rangle \tag{29}$$

To study the coupling between translation and rotation of the particles, we will also consider the rotational diffusivity, defined as

$$D_{\mathrm{R}}(t_n)=\frac{1}{6n\delta t}\left\langle\left(\boldsymbol{\vartheta}(t_n)-\boldsymbol{\vartheta}(t_0)\right)^2\right\rangle \tag{30}$$

$$\boldsymbol{\vartheta}(t_n)=\int_{t_0}^{t_n}\mathrm{d}s\boldsymbol{\Omega}(s) \tag{31}$$

where $\boldsymbol{\vartheta}$ is the unbounded rotational displacement of the particle.

In order to separate the "random" contribution given by the surrounding configuration from the particle's own swimming motion, we consider the displacements within the body frame of reference,

$$\hat{\chi}_i=Q_{i-1}^{t}\Delta_i \tag{32}$$

where tildes are used to denote quantities with respect to the coordinate-system attached to each of the squirmers ($\hat{\boldsymbol{e}}_1,\hat{\boldsymbol{e}}_2,\hat{\boldsymbol{e}}_3$), with $\hat{\boldsymbol{e}}_3$ the preferential swimming axis (see Fig. 3). The advantage of this approach is illustrated in Fig. 4, where the trajectory

of a single particle, from a suspension of pushers $\alpha = +2$ at $\phi = 0.1$, is given in both representations: with respect to the lab- and body-space displacements. One can immediately see where the difficulty in analyzing the particle motion comes from, as the length scales for the directed (swimming) and fluctuating motion differ by an order of magnitude. We define an additional effective hydrodynamic diffusivity $\tilde{D}_{\mathrm{T}}$, in terms of these perpendicular and parallel displacements, as

$$\tilde{D}_{\mathrm{T}}^{\perp}(t_n) = \frac{1}{4n\delta t}\left\langle \left[\sum_{i=1}^{n} \tilde{\Delta}_i^{\perp}\right]^2 \right\rangle \tag{33}$$

$$\tilde{D}_{\mathrm{T}}^{\parallel}(t_n) = \frac{1}{2n\delta t}\left\langle \left[\sum_{i=1}^{n} \tilde{\Delta}_i^{\parallel} - n\delta t U\right]^2 \right\rangle \tag{34}$$

$$\tilde{D}_{\mathrm{T}}(t_n) = \frac{1}{3}\left(2\tilde{D}_{\mathrm{T}}^{\parallel}(t_n) + \tilde{D}_{\mathrm{T}}^{\perp}(t_n)\right) \tag{35}$$

where the second term inside square brackets in eqn (34) is required to remove the (average) contribution to the particle displacements from the inherent swimming motion ($U = \langle \boldsymbol{V}\cdot\hat{\boldsymbol{e}}_3\rangle$ is the average velocity along the particle's swimming axis). These diffusivities provide a direct measure of the strength of the hydrodynamic interactions among the squirmers. The corresponding diffusion coefficients can be obtained from the long-time limit (assuming a plateau has been reached and the limit exists)

$$D_{\mathrm{T}} = \lim_{t\to\infty} D_{\mathrm{T}}(t) \tag{36}$$

$$D_{\mathrm{R}} = \lim_{t\to\infty} D_{\mathrm{R}}(t) \tag{37}$$

$$\tilde{D}_{\mathrm{T}} = \lim_{t\to\infty} \tilde{D}_{\mathrm{T}}(t) \tag{38}$$

Since the parallel and perpendicular effective diffusion coefficients, $\tilde{D}_{\mathrm{T}}^{\parallel}$ and $\tilde{D}_{\mathrm{T}}^{\perp}$, exhibit no deviation from isotropic behavior (although this could be expected to change if persistent long-range order appears), we only consider the average effective diffusion coefficient $\tilde{D}_{\mathrm{T}}$. A similar analysis can be performed for the rotational diffusivities, in order to study the rotations about the three particle axes independently, but it provides no additional information and will not be presented here.

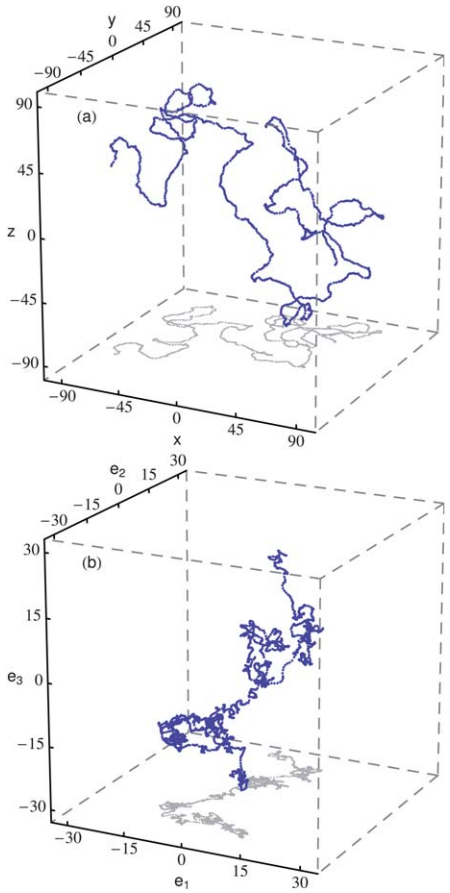

Fig. 4 Trajectory of a single particle in a suspension of pullers $\alpha = +2$ at $\phi = 0.1$. (a) The real lab-space trajectory of the particle, and (b) the body-space trajectory. The latter is constructed by transforming the individual particle displacements to the frame of reference of the particle, and expressing them in terms of displacements parallel and perpendicular to the particle's swimming axis $\hat{\boldsymbol{e}}_3$. In addition, the (parallel) motion due to the average swimming speed, $\Delta x(t) = \langle \boldsymbol{V}\cdot\hat{\boldsymbol{e}}_3\rangle t$, has been removed. Thus, (b) gives the random motion induced on the particle by the local fluctuations in the surrounding flow field. The length scale is given by the particle radius $a/\Delta = 5$ and the projections of the trajectories onto the bottom plane have been added as a visual guide.

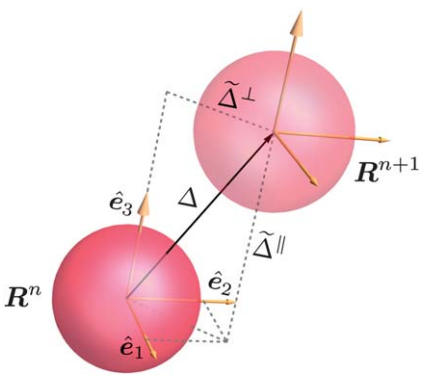

Fig. 3 Analysis of the particle displacements with respect to the particle's moving coordinate frame. The particle displacement Δ during a given time interval is decomposed into its components parallel $\hat{\chi}^{\parallel}$ and perpendicular $\hat{\chi}^{\perp}$ to the swimming axis. For a single isolated squirmer $\hat{\chi}^{\perp} = 0$ for any given time interval; for a suspension of swimmers the flow induced by the neighboring particles gives rise to non-zero perpendicular displacements.

Finally, we also consider the velocity auto-correlation functions[52]

$$C_V(t) = \langle \boldsymbol{V}(t)\cdot\boldsymbol{V}(t_0)\rangle \tag{39}$$

$$C_{\Omega}(t) = \langle \boldsymbol{\Omega}(t)\cdot\boldsymbol{\Omega}(t_0)\rangle \tag{40}$$

and in particular, the correlation functions for the velocity components parallel and perpendicular to the swimming axis

$$C_V^{\parallel}(t) = \langle \boldsymbol{V}^{\parallel}(t)\cdot\boldsymbol{V}^{\parallel}(t_0)\rangle \tag{41}$$

$$\tilde{C}_V^{\parallel}(t) = \langle \tilde{\boldsymbol{V}}^{\parallel}(t)\cdot\tilde{\boldsymbol{V}}^{\parallel}(t_0)\rangle \tag{42}$$

$$\tilde{\boldsymbol{C}}_V^{\perp}(t) = \langle \tilde{\boldsymbol{V}}^{\perp}(t)\cdot\tilde{\boldsymbol{V}}^{\perp}(t_0)\rangle \tag{43}$$

Although eqn (41) and (42) both measure the correlations of the parallel velocity components, the former does so within the fixed lab frame, while the latter uses the moving body frame. Therefore, the first will be sensitive to changes in the magnitude and direction of the velocity vector, while the second will only register changes in the magnitude. At short times, we can expect the decay in correlations of the parallel velocity components to be determined by the local configuration of the suspension (where the flow generated by the nearby particles can act to enhance or suppress the swimming motion), and at long times by the particle collisions, which will reorient the particle's swimming direction. This means the initial decay should be the same for both $C_V^{\parallel}$ and $\tilde{C}_V^{\parallel}$, since the particle has not had time to reorient itself; at long times however, correlations measured within the lab frame of reference should decay to zero, whereas those measured within the body reference should reach a finite value (determined by the average swimming speed of the squirmers). For the decay in correlations of the perpendicular velocity components $\tilde{C}_V^{\perp}$ we expect a behavior analogous to the short-time decay of the parallel components, since it is due entirely to the flow field generated by the neighboring squirmers. We note that a similar analysis has been successfully used to study the interplay between hydrodynamic and Brownian fluctuations on the motion of (inert) sedimenting colloids.[53]

3 Validation

The first obvious test of our simulation method is to make sure that an isolated swimmer will move at the expected velocity $U = 2/3B_1$, regardless of the particle size or the value of the second squirming mode B_2. We performed simulations for a single squirmer, inside a periodically replicated cubic simulation box of dimension $L = 128\Delta$ (Δ is the grid spacing), for various particles sizes and squirming modes. Fig. 5 shows the results obtained for a neutral squirmer ($\alpha = 0$), for particle sizes $a/\Delta = 4, 5, 6, 8$, and for various pullers ($\alpha > 0$), with a particle size of $a/\Delta = 6$. The particle Reynolds number $\mathrm{Re} = \rho U a/\eta$ and the width of the diffuse interface ζ/Δ were the same for all the simulations, 0.01 and 2, respectively. In all cases, the particle's (average) swimming velocity shows excellent agreement with the theoretical predictions. For the neutral squirmers, the swimming velocity is within $\simeq 2\%$ of the exact value, regardless of the particle diameter, although the speed shows a small decrease with increasing particle size. The small oscillations exhibited by the velocity are due to discretization errors, as the number of grid points on the two hemispheres of the particle surface will vary depending on the relative position of the particle center within the computational bins. Similar agreement is obtained for the pullers (pushers), although the discretization error increases with increasing $|\alpha|$ (at fixed particle size a/Δ). As such, for the system sizes we have considered, we are limited to moderate values of $|\alpha| \lesssim 5$.

To verify that the velocity field generated by our SP squirmers is correct, we compare with the exact (at $\mathrm{Re} = 0$) analytical expression given in eqn (3). The steady-state velocity fields generated by a single squirmer ($L/\Delta = 128, A/\Delta = 6, \zeta/\Delta = 2, \alpha = +2, \mathrm{Re} = 0.01$), along with the corresponding stream line plot (in the lab and particle reference frames), are shown in Fig. 6. Excellent agreement with the analytical results is obtained, although differences in the stream lines arise at large distances $r/a \simeq 4$ for $\theta \simeq \pm\pi/4$ (with respect to the swimming axis $+\hat{z}$). Even though the fluid velocity within these regions is vanishingly small (compared to the swimming speed of the squirmer), a clear systematic deviation is observed in the direction of the stream lines. This is due to our use of periodic boundary conditions, which causes the stream lines to close in on themselves, in order to match at the boundaries of the simulation cell. A similar deviation is observed for the velocities along the swimming direction, but these occur at much larger distances.

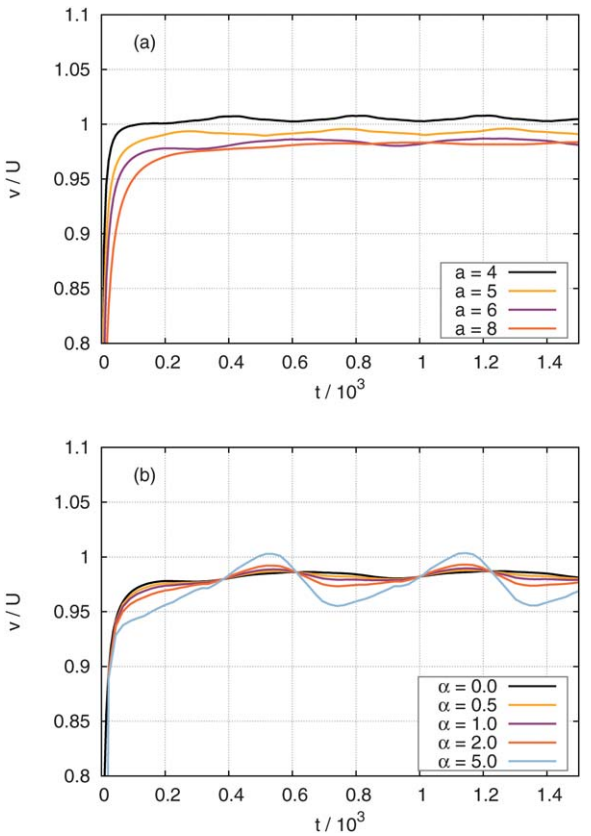

Fig. 5 Swimming speed of an isolated squirmer in a periodically replicated cubic simulation box of length $L/\Delta = 128$ at $\mathrm{Re} = 0.01$ as a function of time (in simulation units). (a) Neutral swimmer at various particle sizes a/Δ. (b) Puller of size $a/\Delta = 6$ for various swimming modes $0 \leq \alpha \leq 5$. Velocities are scaled by the theoretical value for the swimming speed $U = 2/3B_1$.

Following Götze and Gompper,[46] we consider the interactions between two fixed squirmers at a distance r from each other, with parallel orientations. Fig. 7 shows the results we have obtained for the force parallel to the displacement vector between two pullers (perpendicular to their swimming axes), normalized by the Stokes force $F_S = 6\pi\eta a U$ for an inert particle moving with the same velocity ($U = 2/3B_1$). The simulations were carried out at $\mathrm{Re} = 0.01$ for a box size of $L/\Delta = 128$, with a particle radius of $a/\Delta = 6$, and a swimming mode $\alpha = +2$. The functional form for this perpendicular force has been given by Ishikawa *et al.*[33]

$$F_{\mathrm{near}} \propto \log(\varepsilon) \tag{44}$$

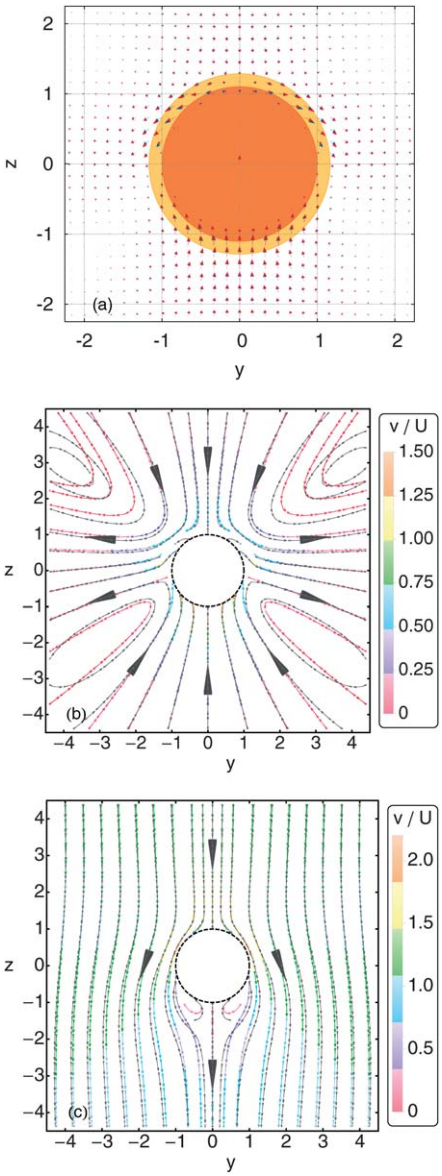

Fig. 6 Azimuthally averaged steady-state fluid velocities for a single puller $\alpha = +2$ of size $a/\Delta = 6$ swimming along the $\hat{z}$-axis, within a periodically replicated cubic simulation box of size $L/\Delta = 128$. (a) Fluid velocity vectors within the laboratory frame, the red and blue arrows show the simulation and analytical results, respectively. (b) Fluid velocity stream lines within the laboratory frame, the colored lines (color-coded with respect to the magnitude of the velocity) represent the analytical solution, while the gray lines show the simulation results. (c) Same as (b) but within a reference frame moving with the particle. Due to discretization errors, streamlines can begin/end at the fluid–particle interface. Length scales have been scaled by the particle radius.

where $\varepsilon = r - \sigma$ is the minimum separation distance between the surface of the particles (with $\sigma = 2a$ the particle diameter). Additionally, they also obtained exact far-field expressions for the force between the two squirmers from a generalization of Faxen's laws,

$$F_{\text{far}} = \frac{3\,\pi\sigma^3\alpha\,B_1}{16r^2} \tag{45}$$

At short distances the repulsive force experienced by the two squirmers is seen to follow the expected scaling relationship up

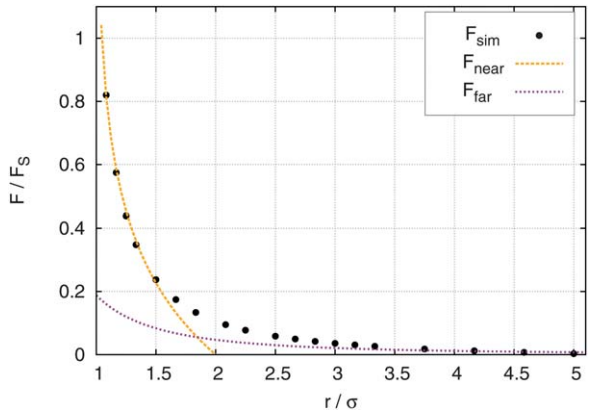

Fig. 7 Perpendicular force felt by two (fixed) parallel squirmers ($\alpha = +2$), of diameter $\sigma/\Delta = 10$ and interface thickness $\zeta/\Delta = 2$, as a function of distance r, for $\text{Re} = 0.01$ and a system size of $L/\Delta = 128$. The dashed (yellow) line gives the fit to the expected functional form $F/F_s = A\ln(r/\sigma - 1)$ of the near-field force, with $A = -0.327$, while the dotted (violet) line gives the (exact) far-field force. All forces are normalized by the Stokes force for an inert sphere with the same speed ($U = 2/3B_1$).

to $r \lesssim 1.5\sigma$, while the far-field force is approached asymptotically for $r \gtrsim 3\sigma$. The force is observed to be proportional to the swimming mode, such that $F \propto \alpha$ and $\boldsymbol{F}(\alpha) = -\boldsymbol{F}(-\alpha)$.

4 Results and discussions

4.1 Diffusion coefficients

We have studied the diffusive behavior of a semi-dilute suspension of identical non-buoyant squirmers, for various concentrations $\phi \leq 0.124$ (with $\phi = 4\pi a^3 N/3V$ the packing fraction) and squirming modes $\alpha = 0, \pm 1, \pm 2$. We work in reduced units, in which the density and viscosity of the host fluid are unity $\rho = \mu = 1$. All simulations were performed for squirmers of radius $a/\Delta = 5$ (interface width $\zeta/\Delta = 2$), in a cubic simulation box of length $L/\Delta = 64$, for a particle Reynolds number of $\text{Re} = \rho U a/\mu = 0.05$ (U is the swimming speed of an isolated squirmer). Although our systems are not very large $L/a \sim 12$, finite size effects have been shown to be small,[28] and since we will be mainly focused on studying the short-range hydrodynamic interactions among particles, they can be safely ignored. In what follows, all quantities are presented in non-dimensionalized form, using as characteristic length, speed, and time units the particle radius a, swimming speed $U = 2/3B_1$, and the time required for an isolated squirmer to move a distance equal to its radius $T = a/U$.

The diffusivities $D_{\text{T}}(t)$ and $\tilde{D}_{\text{T}}(t)$, defined in eqn (29) and (35), for a system of pullers ($\alpha = +2$), at various concentrations, are shown in Fig. 8. The standard diffusivities $D_{\text{T}}(t)$ show a ballistic regime which extends to very long times $t \simeq 100$, after which the slope starts to decrease, indicating a transition towards a diffusive regime. However, purely diffusive motion (slope of zero) is only obtained for the highest concentrations and alpha values. This behavior has been analyzed in detail in ref. 28. In contrast, $\tilde{D}_{\text{T}}(t)$ reaches the diffusive regime at much shorter times, for all concentrations and all non-zero values of alpha. We note that both quantities are measuring related

phenomena, but the latter does so directly, since the motion due to the inherent particle swimming has been removed from the analysis. As a function of concentration, $\tilde{D}_T$ shows a clear increase, which is consistent with the interpretation of the diffusive motion being caused by interactions with neighboring particles: as the concentration increases, so does the number of neighbors, and thus the strength of the interactions. In contrast, we see that D_T decreases with concentration. The reason for this is simple, since D_T mainly measures the effect of the particles' own swimming, an increase in the diffusive behavior can only hinder this motion. The rotational diffusivities D_R, also shown in Fig. 8, present the same basic features as $\tilde{D}_T$, the onset of the diffusive regime is obtained within the same time interval and they exhibit a similar concentration dependence. Apart from a difference in scale, there is no clear differentiating factor between these two quantities. Similar results are obtained for all other non-zero values of α considered; where, as was pointed out by Ishikawa and Pedley,[28] the effect of increasing (decreasing) α is the same as that of increasing (decreasing) the concentration, at least with respect to the diffusive motion of the squirmers, since they both lead to an increase (decrease) in the strength of the hydrodynamic interactions among particles.

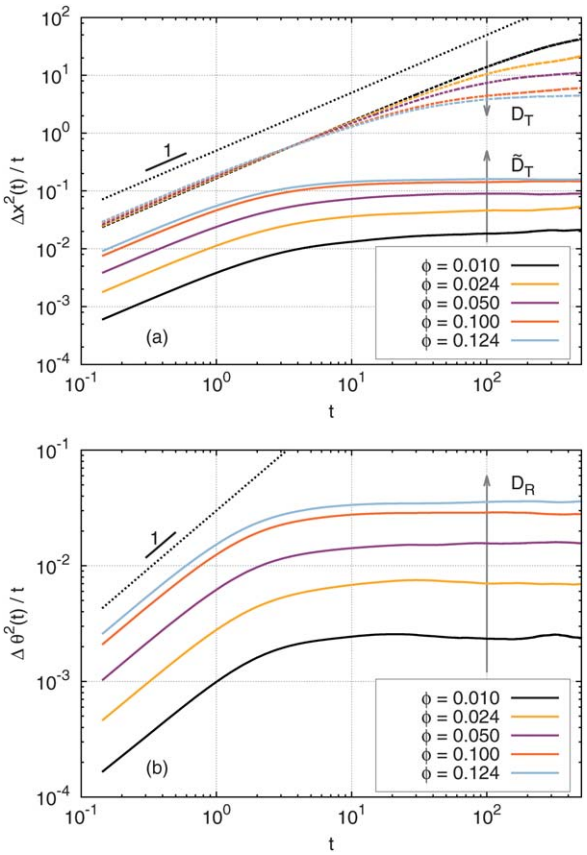

Fig. 8 Translational and rotational diffusivities for a system of pullers ($\alpha = +2$) at various concentrations. (a) Translational diffusivities obtained from the mean-squared displacements in the fixed-lab reference frame $D_T(t)$, and the body frame $\tilde{D}_T(t)$ (with the displacement due to the intrinsic swimming motion suitably removed), dashed and solid lines, respectively; and (b) the rotational diffusivities $D_R(t)$. Lines of slope one, corresponding to purely ballistic motion, have been drawn for comparison. The arrows show the increase/decrease of the various diffusivities as a function of concentration ϕ.

4.2 Velocity fluctuations and correlations

To have a better understanding of the how the diffusive motion arises, we now consider the single particle velocity correlation functions defined in eqn (39)–(43). We present in detail the results obtained for a system of pullers ($\alpha = +2$) at $\phi = 0.124$, shown in Fig. 9, but the same analysis applies for the other values of $\phi(\alpha)$ we have studied. The standard definition of the velocity auto-correlation $C_V(t)$ results in a function that shows a two-time decay process, as evidenced by the shoulder that appears around $1 < t < 10$. The initial decay ($t \simeq 1$) is due to the changing configuration of neighboring particles (and their self-generated flow field), while the second, long time decay ($t \simeq 10$) arises due to the reorientation of the particles' swimming direction, which is a consequence of the particle–particle collisions. Confirmation for this interpretation is provided by the three other correlation functions we have defined. Consider first the decay in correlations of the parallel velocity components, $C_V^{\parallel}(t)$ (lab frame) and $\tilde{C}_V^{\parallel}$ (particle frame). Both functions show the same initial decay, caused by local fluctuations in the velocity field, as the particle has not experienced any significant change in its swimming direction. However, at longer times, these two functions show a completely different behavior. The parallel correlations measured within the fixed lab system $C_V^{\parallel}(t)$ exhibit a slow (long-time) decay before eventually collapsing onto the full correlation function $C_V(t)$; the deviations at long times $t > 50$ are due to statistical uncertainties in our data. In contrast, the correlations measured within the particle's frame of reference reach a plateau after the initial decay. This means that while the particle is constantly reacting to the flow field generated by its neighbors, by changing it's swimming speed, these fluctuations decay very fast, typically within the time it takes for the particle to travel its diameter (the characteristic

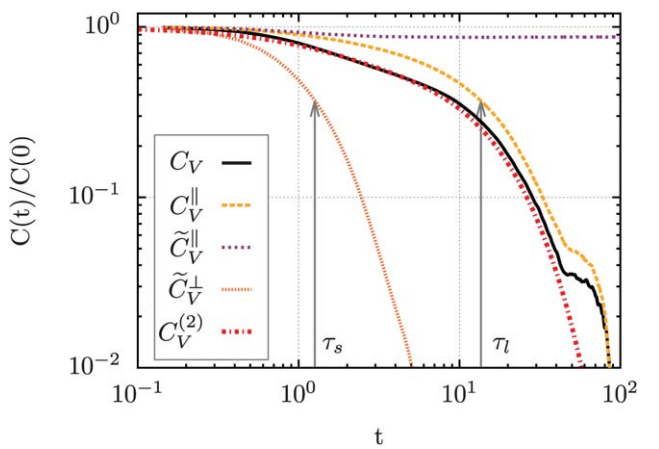

Fig. 9 Single-particle velocity time-correlation functions for a system of pullers ($\alpha = +2$) at $\phi = 0.124$. The two-time relaxation approximation to the velocity correlation function $C_V^{(2)}(t)/C_V(0)$ (eqn (46)), with the amplitudes and relaxation times obtained from the simulation, is also shown (dash-dot red line).

length over which the flow field varies significantly). As such, the long-time decay in both $C_V(t)$ and $\tilde{C}_V^{\parallel}(t)$ is due primarily to changes in the orientation of the swimming direction, and not to changes in the magnitude of the swimming speed. As expected, the correlations in the perpendicular velocities $\tilde{C}_V^{\perp}(t)$ show a very fast decay, over a characteristic time equal to that of the initial short-time decay of the parallel velocity components. The decay in correlations of the angular velocity $C_\Omega(t)$ (not shown) presents the same characteristic behavior as $\tilde{C}_V^{\perp}(t)$.

Finally, the characteristic times τ_s and τ_l for these two processes, governed by the hydrodynamic interactions and the particle collisions, can be obtained by assuming an exponential decay $\exp(-t/\tau)$ for the appropriate correlation function: $\tilde{C}_V^{\perp}(t)$ and $C_V^{\parallel}(t)$ for τ_s and τ_l, respectively (see Fig. 9). The two-time scale relaxation of the velocity fluctuations can then be approximated as

$$\begin{aligned} C_V^{(2)}(t;\phi,\alpha) &= \chi_s(\phi,\alpha)\mathrm{e}^{-t/\tau_s(\phi,\alpha)} + \chi_l(\phi,\alpha)\mathrm{e}^{-t/\tau_l(\phi,\alpha)} \\ \chi_s &= \langle \delta\boldsymbol{V}\cdot\delta\boldsymbol{V}\rangle \\ \chi_l &= U_{\parallel}{}^2 \end{aligned} \tag{46}$$

with $U_{\parallel} = \langle \boldsymbol{V}\cdot\hat{\boldsymbol{e}}_3\rangle$ and where we have explicitly shown the dependence of the amplitudes χ and decay times τ on the concentration and swimming mode of the particles. Fig. 9 shows excellent agreement between this two-time relaxation process (with all four parameters obtained from the simulation data) and the full correlation function $C_V(t)$ defined in eqn (39). Furthermore, in what follows we show how the long-time decay can be simplified and interpreted in terms of a binary collision process between the swimmers.

4.3 Scaling

To confirm the interpretation we have given for the diffusive motion of the squirmers, and the emergence of the two time-scales, we perform a scaling analysis for the relevant parameters (diffusion coefficients and collision time scales), as a function of concentration ϕ. Although a similar analysis has been presented in ref. 28 by Ishikawa and Pedley, they have not considered the effective diffusion $\tilde{D}_T$, which means that only the long-time behavior of the system, given by the particle collisions, was analyzed (the hydrodynamic interactions which give rise to the rapidly decaying velocity fluctuations are completely masked by the swimming motion). In a subsequent study,[31] the authors considered the diffusion of fluid particles, as well as inert colloidal particles, in a suspension of swimmers, and in this case they were able to observe the emergence of a second (shorter) time-scale. Our results, which are in agreement with their scaling arguments, provide a complementary view of the diffusive motion of these squirmer systems. The benefit of the analysis we propose lies in the fact that all relevant time and length scales can be obtained just from the motion of the squirmers, *i.e.*, there is no need to consider the motion of the fluid or to introduce inert (non-swimming) particles. This results in simpler simulations and will also be relevant when trying to compare with experimental data.

4.3.1 Correlation times. First, lest us consider the long-time dynamics of the system, which is determined by the particle–particle collisions of the swimmers. From the kinetic theory of gases,[54] we know that the mean free path λ (or average distance between collisions) should be proportional to the inverse of the concentration of particles. In reduced units, we have

$$\lambda = \frac{2\sqrt{2}}{3}\left(\sigma_c{}^2\phi\right)^{-1} \tag{47}$$

with ϕ the packing fraction, and σ_c the collision or cross-section diameter, which is not necessarily equal to the actual physical diameter of the particle. This difference is due to the self-generated flow profile around each particle, and as such should only depend on the swimming mode α, not on the concentration of particles. For the moment though, let us assume that we are dealing with hard-spheres $\sigma_c = 2$, the average time between collisions is simply $t_c^{HS} = \lambda^{HS}/U_c$, which gives

$$t_c^{HS} = \frac{\sqrt{2}}{6}\left(U_c\phi\right)^{-1} \tag{48}$$

where U_c is the average velocity of the particles. In thermal systems, this velocity would be determined by the reservoir and be independent of concentration, so that one obtains the well known ϕ^{-1} dependence for the collision time $t_c^{HS} \propto \phi^{-1}$. Although the velocity of our squirmers is not concentration independent, to first order, we can safely assume that the particles are all swimming at an average velocity which is near the swimming velocity of an isolated squirmer, $U_c = 1$. Therefore, the collision time for our systems should show the same concentration dependence predicted by kinetic theory, $t_c \propto \phi^{-1}$. To obtain the collision times t_c from the decay times τ computed from the simulations, we use the Enskog approximation[52,54]

$$t_c = 2\tau/3 \tag{49}$$

Our results, shown in Fig. 10, confirm the scaling predictions for the long-time decay $t_c^l = 2\tau_l/3$. Of special interest is the difference between t_c^l for the different squirming modes, with the collision time decreasing with increasing α. This can be explained by an increase in the effective size of the particle, as the mean free path λ is inversely proportional to the collision diameter σ_c. We also show the mean collision time t_c^{HS} for an equivalent system of hard-spheres. The fact that the collision times for the squirmers are significantly larger than the corresponding hard-spheres values is surprising, since it implies that the squirmers have a cross-section diameter which is smaller than the hard-sphere diameter of the particle ($t_c \propto \sigma_c{}^{-2}$). The reason for this lies in the collision dynamics of the squirmers.

The scaling of the fast time-scale τ_s (or t_c^s) is harder to elucidate, since it shows only a very weak concentration dependence. Given that τ_s is related to the velocity fluctuations caused by the short-range hydrodynamic interactions between particles, it should be related to the time it takes for the flow region around a particle to change: this is essentially the time necessary for a particle to swim its diameter $t \simeq 2$. Our results, also shown in Fig. 10, agree with this rough estimate and also indicate a power-law behavior with an exponent of $\simeq -1/6$.

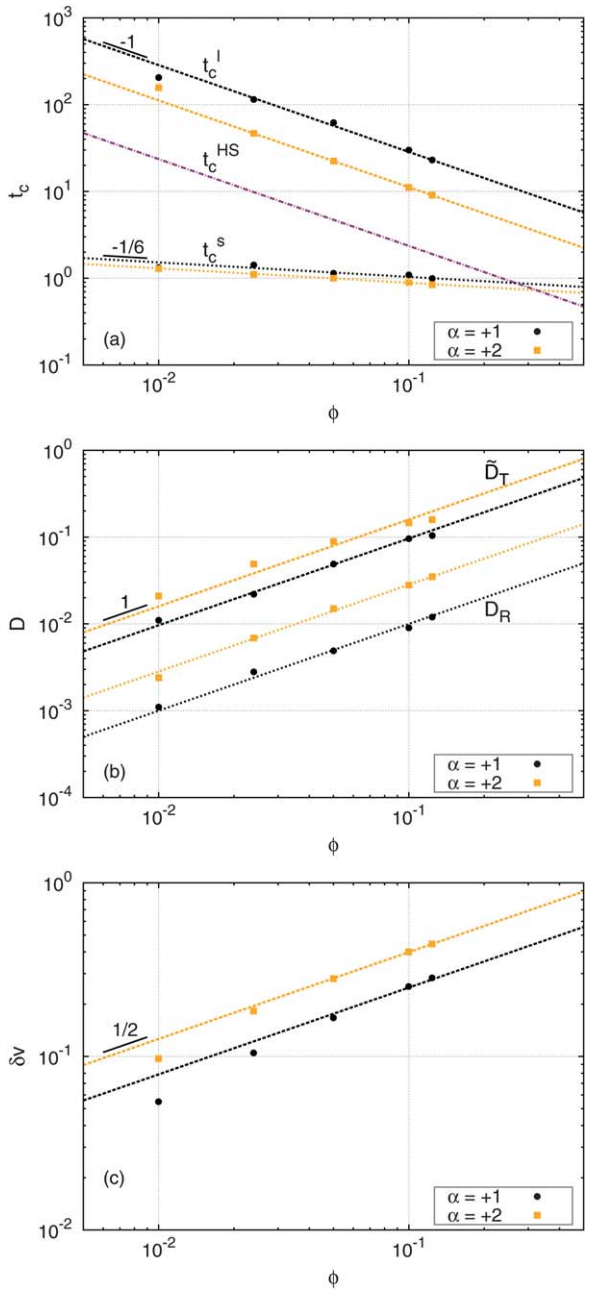

Fig. 10 (a) Scaling of the collision times, t_c^I and t_c^S, with concentration ϕ. Also shown is the collision time t_c^{HS} for an equivalent system of hard spheres, with a (scaled) velocity of $U_c = 1$, given by the kinetic theory of gases. (b) Scaling of the translational $\tilde{D}_T$ and rotational D_R diffusion coefficients with concentration. (c) Scaling of the velocity fluctuations with concentration.

Although the decrease with concentration seems clear, it is very difficult to accurately measure such small variations and we have no suitable explanation for the value of this exponent (given by a fit to the data). These results are analogous to those obtained by Ishikawa *et al.*[31] for the time-scale of diffusing fluid particles in a suspension of squirmers.

4.3.2 Diffusion coefficients. For the scaling of the translational diffusion coefficients, a simple dimensional analysis yields

$$D_T \propto U_c^2 t_c \tag{50}$$

where U_c and t_c are the characteristic velocity and time scales of the collision process which gives rise to the diffusive motion.[31] For the standard diffusion coefficient D_T (eqn (36)), the reorientation of the particles is caused by the particle–particle collisions, thus $t_c = t_c^I$ and $D_T \propto \phi^{-1}$ (assuming a constant swimming velocity). This behavior has been analyzed in detail in ref. 28. More relevant to our study is the scaling of the effective diffusion coefficient $\tilde{D}_T$ (eqn (38)), in which the motion due to the particle swimming has been removed. Our results, shown in Fig. 10, indicate a linear dependence with concentration $\tilde{D}_T \propto \phi$. This is precisely the scaling behavior reported by Ishikawa *et al.*[31] for the diffusion of inert/fluid particles, and the same concentration dependence that has been observed experimentally for the diffusion of tracer particles in swimming suspensions (for both pushers and pullers).[29,30] This is not surprising, since we can consider that this diffusive motion arises due to collisions between the particle (swimmer or not) and the fluid. By definition, it is clear that the velocity and time scales cannot be the same swimming speed or collision time used to define D_T. In this case, the characteristic velocity scale will be set by the velocity fluctuations δv around the average swimming velocity, which can be directly measured by computing the velocity components perpendicular to the swimming axis of the particles $V^{\perp}$. For these fluctuations, our simulations indicate a square-root dependence with concentration $\delta v \propto \sqrt{\phi}$ (see Fig. 10). The characteristic time-scale for this process will be the time necessary for the fluid flow surrounding a given particle to show considerable variations, and this can be estimated by the time it takes the particle to travel its own diameter $t_c \propto 1$. We thus recover the linear dependence given by the simulations. The same scaling behavior is obtained for the rotational diffusion coefficient $D_R \propto \phi$.

4.3.3 Collision diameters. So far, we have not considered the effect of the squirming mode α on the diffusive properties of the swimmers. While it is clear that increasing the magnitude of α will give rise to stronger hydrodynamic interactions, and thus increase the diffusion of the particles (as can be seen in Fig. 10), it is not clear how this dependence can be quantified. We propose that α, which defines the strength/range of the self-generated fluid-flow around a squirmer (eqn (3)), can be directly related to the effective collision diameter of the swimmers. From the expression of the mean free path, eqn (47), we obtain the following for the collision radius $r_c = \sigma_c/2$

$$r_c = \left(3\sqrt{2} U_c t_c \phi\right)^{-1/2} \tag{51}$$

Assuming $t_c = f(\alpha)\phi^{-1}$, with $f(\alpha)$ a function only of the squirming mode α, and considering the swimming velocity to be constant ($U_c = 1$), we arrive at a concentration independent collision radius

$$r_c \propto [f(\alpha)]^{-1/2} \tag{52}$$

As $f(\alpha)$ is a decreasing function of α, the effective collision radius of the particle should increase with the magnitude of the squirming mode. Our results for the collision radius, given by

eqn (51), with $U_c = U_{\|} = \langle \boldsymbol{V}\cdot\hat{\boldsymbol{e}}_3\rangle$ and $t_c = 2/3\tau^1$ obtained directly from the simulations, are shown in Fig. 11. Allowing for the large uncertainties in measuring the decay times at low concentrations, we obtain very good agreement with the previous scaling analysis: the radii show only a small variation with ϕ, and a clear distinction is observed as $|\alpha|$ is increased. We note however that the pushers seem to present a larger collision radius than the pullers, something which is difficult to explain with the simple collision model we have presented.

Also shown in Fig. 11 is the mean collision radius r_c as a function of α. Although more data is needed to accurately specify the functional form of $f(\alpha)$, a simple linear dependence predicts a value of r_c ($\alpha = 0$) which is an order of magnitude smaller than the hard-sphere radius of the particles $r_c \simeq 0.1$. This is consistent with our simulations, from which we were unable to obtain reliable estimates for τ_l, because the velocity correlation functions exhibited no substantial decay over the time scales we studied $t \simeq 10^2$ to 10^3. However, we were able to obtain estimates for the effective diffusion coefficients $\tilde{D}_T$ of these neutral squirmers, which are an order of magnitude smaller than the corresponding values for $\alpha = +1$. This means that the difference in collision times, with respect to a corresponding system of hard-spheres (see Fig. 10), will be even larger for the neutral squirmers than it is for the swimmers with non-zero α values. This is consistent with an interpretation in terms of hard-spheres when analyzing the differences among squirmers (larger α equivalent to larger collision radius r_c), but it can appear contradictory when comparing to actual hard-sphere systems. After all, we could expect the systems for $\alpha = 0$, in which the flow profile due to the squirming motion is most localized ($U(r) \propto r^{-3}$), to be closest to a system of hard-spheres. Yet our results indicate that the collision radius of the neutral squirmers is an order of magnitude smaller than the actual radius of the particles. As we have already mentioned, this is due to the difference in the collision dynamics of the particles, which differ dramatically from that of hard-spheres.[33,55] Although the exact collision process will depend not only on the relative velocity of the particles, but also on their relative orientations, the squirming motion results in deflection angles which are (on average) smaller than the corresponding hard-sphere values. In essence, this means that the flow fields generated by the particles allows them to swim past each other with a relatively small change in their swimming direction (again, as compared with an actual hard-sphere collision).

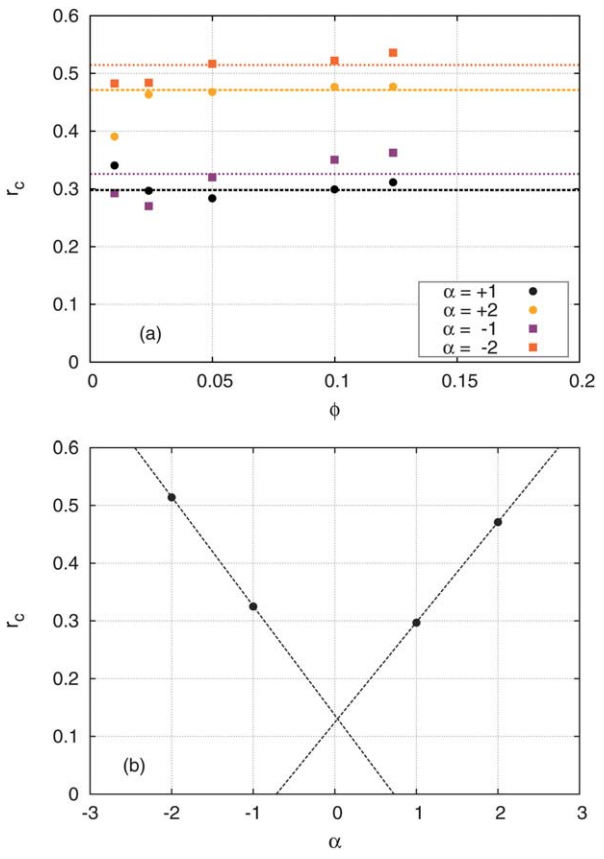

Fig. 11 Effective collision radius r_c of the squirmers as a function of (a) concentration ϕ and (b) swimming mode α. Results were obtained by using the mean free path expression for a system of hard-spheres given by the kinetic theory of gases eqn (51), with the velocity and collision time given by the simulation data.

Finally, using eqn (51), the velocity correlation function for a suspension of squirmers (eqn (46)) can be reduced to the following functional form

$$C_V(t;\phi,\alpha) = \chi_s e^{-t/\tau_s} + U_{\|}{}^2 e^{-\sqrt{2}\sigma_c U_{\|}\phi t} \quad (53)$$

where the long-time decay process is expressed only in terms of the average swimming speed $U_{\|}(\phi, \alpha)$ and the hard-sphere collision diameter $\sigma_c(\alpha)$ of the squirmers. The former has a weak linear dependence on concentration $U_{\|} = 1 - A(\alpha)\phi$, while the latter is concentration independent, as was shown in Fig. 11. The scaling behavior for the short time process is still not understood, but a fit to our simulation results suggest a power law behavior for the concentration dependence of the amplitude and decay time of the velocity fluctuations, with an exponent of 1/2 and −1/6, respectively; *i.e.*, $\chi_s \propto \phi$ and $\tau_s \propto \phi^{-1/6}$. A more detailed analysis is required to firmly establish these scaling relationships, as well as to determine the dependence on the swimming parameter α. Work along these lines is in progress.

5 Conclusions

We have investigated the hydrodynamic interactions of suspensions of squirmers using a modified version of the smoothed profile method (SP) for particle dispersions. The SP method allows one to fully resolve the hydrodynamic interactions in many particle dispersions in an accurate and efficient manner, and we have shown how it can be extended to systems with slip boundary conditions, such that it is possible to describe squirmers (active swimmers which move due to self-generated surface tangential velocities). The validity of the method was confirmed by comparing the simulation data with exact results for the case of a single swimmer, for which we recover the correct swimming speed and are able to accurately reproduce the fluid flow generated by the squirming motion, and for two aligned swimmers at a fixed distance, for which we recover the expected hydrodynamic force. The advantage of the

SP method for swimming particles, as opposed to Stokesian Dynamics (which has been successfully, and extensively, used to study these systems) is its applicability to particle dispersions in complex fluids. This is relevant in the case of swimming microorganisms, since the role of the nutrient and the possibility of having a non-Newtonian host fluid must be considered when comparing with experiments.

In this paper we have analyzed the effect of the hydrodynamic interactions on the motion of semi-dilute squirmer suspensions, up to volume fractions of $\phi = 0.124$, for various swimming modes $|\alpha| \leq 2$. Although we have no yet included thermal fluctuations in our description, the swimming motion of the particles gives rise, over sufficiently long time scales, to a diffusive regime. In order to distinguish between the contributions due to the hydrodynamic interactions, caused by the squirming motion, and those due to the particle–particle collisions, which are the two basic mechanisms responsible for the diffusive motion, we have analyzed the particle dynamics in terms of movement due to the inherent swimming of the particles, and that due to the (hydrodynamic) interactions among them. This is easily done by looking at the motion from the particle's own frame of reference, *i.e.*, decomposing the motion parallel and perpendicular to the swimming axis. This analysis has allowed us to demonstrate the appearance of two distinct time scales within our system, one related to the time between particle–particle collisions, the other to the fluid–particle interactions. This two-time scale nature of the particle interactions in swimming suspensions can be clearly seen in the two-time relaxation of the velocity correlation function. We are thus able to define an effective hydrodynamic diffusion coefficient (corresponding to the short-time fluid–particle interactions), in which the self-motion of the particle has been removed, which shows a linear scaling with concentration. In contrast, the standard diffusion coefficient is inversely proportional to the concentration of swimmers. This is in agreement with simulation and experimental results on tracer diffusion in swimming suspensions. Additionally, since the long-time dynamics of the system is related to the particle–particle collisions, we have used the well-known results from kinetic theory to deduce an effective, concentration independent, collision radius for our swimmers. Due to the complex collision dynamics of these particles, this collision radius is actually smaller than the hard-sphere radius of the particle, and increases with increasing α.

Acknowledgements

The authors would like to express their gratitude to the Japan Society for the Promotion of Science for financial support (Grants-in-Aid for Scientific Research KAKENHI no 23244087).

References

1 E. M. Purcell, *Am. J. Phys.*, 1977, **45**, 3–11.
2 E. Lauga and T. R. Powers, *Rep. Prog. Phys.*, 2009, **72**, 096601.
3 M. Manghi, X. Schlagberger, Y.-W. Kim and R. R. Netz, *Soft Matter*, 2006, **2**, 653–668.
4 R. Golestanian, J. M. Yeomans and N. Uchida, *Soft Matter*, 2011, **7**, 3074–3082.
5 J. S. Guasto, R. Rusconi and R. Stocker, *Annu. Rev. Fluid Mech.*, 2012, **44**, 373–400.
6 S. Ramaswamy, *Annu. Rev. Condens. Matter Phys.*, 2010, **1**, 323–345.
7 D. L. Koch and G. Subramanian, *Annu. Rev. Fluid Mech.*, 2011, **43**, 637–659.
8 T. Ishikawa and T. J. Pedley, *J. Fluid Mech.*, 2007, **588**, 399–435.
9 A. Sokolov and I. S. Aranson, *Phys. Rev. Lett.*, 2009, **103**, 148101.
10 S. Rafaï, L. Jibuti and P. Peyla, *Phys. Rev. Lett.*, 2010, **104**, 098102.
11 G. K. Batchelor, *J. Fluid Mech.*, 1970, **41**, 545–570.
12 A. Sokolov, I. S. Aranson, J. O. Kessler and R. E. Goldstein, *Phys. Rev. Lett.*, 2007, **98**, 158102.
13 K. Drescher, K. C. Leptos, I. Tuval, T. Ishikawa, T. J. Pedley and R. E. Goldstein, *Phys. Rev. Lett.*, 2009, **102**, 168101.
14 J. Toner, Y. Tu and S. Ramaswamy, *Ann. Phys.*, 2005, **318**, 170–244.
15 J. L. Anderson, *Annu. Rev. Fluid Mech.*, 1989, **21**, 61–99.
16 W. F. Paxton, S. Sundararajan, T. E. Mallouk and A. Sen, *Angew. Chem., Int. Ed.*, 2006, **45**, 5420–5429.
17 W. F. Paxton, A. Sen and T. E. Mallouk, *Chem.–Eur. J.*, 2005, **11**, 6462–6470.
18 J. R. Howse, R. A. L. Jones, A. J. Ryan, T. Gough, R. Vafabakhsh and R. Golestanian, *Phys. Rev. Lett.*, 2007, **99**, 048102.
19 H.-R. Jiang, N. Yoshinaga and M. Sano, *Phys. Rev. Lett.*, 2010, **105**, 268302.
20 L. Baraban, M. Tasinkevych, M. N. Popescu, S. Sanchez, S. Dietrich and O. G. Schmidt, *Soft Matter*, 2012, **8**, 48–52.
21 G. V. Kolmakov, V. V. Yashin, S. P. Levitan and A. C. Balazs, *Soft Matter*, 2011, **7**, 3168–3176.
22 W. Yang, V. R. Misko, K. Nelissen, M. Kong and F. M. Peeters, *Soft Matter*, 2012, **8**, 5175–5179.
23 R. Golestanian, T. B. Liverpool and A. Ajdari, *New J. Phys.*, 2007, **9**, 126.
24 J. F. Brady, *J. Fluid Mech.*, 2011, **667**, 216–259.
25 M. J. Lighthill, *Annu. Rev. Fluid Mech.*, 1969, **1**, 413–446.
26 J. R. Blake, *J. Fluid Mech.*, 1971, **46**, 199–208.
27 Y. Nakayama and R. Yamamoto, *Phys. Rev. E: Stat., Nonlinear, Soft Matter Phys.*, 2005, **71**, 036707.
28 T. Ishikawa and T. J. Pedley, *J. Fluid Mech.*, 2007, **588**, 437–462.
29 M. J. Kim and K. S. Breuer, *Phys. Fluids*, 2004, **16**, L78.
30 K. Leptos, J. Guasto, J. Gollub, A. Pesci and R. Goldstein, *Phys. Rev. Lett.*, 2009, **103**, 198103.
31 T. Ishikawa, J. T. Locsei and T. Pedley, *Phys. Rev. E: Stat., Nonlinear, Soft Matter Phys.*, 2010, **82**, 021408.
32 A. Sokolov and I. S. Aranson, *Phys. Rev. Lett.*, 2012, **109**, 248109.
33 T. Ishikawa, M. P. Simmonds and T. J. Pedley, *J. Fluid Mech.*, 2006, **568**, 119–160.
34 L. Zhu, E. Lauga and L. Brandt, *Phys. Fluids*, 2012, **24**, 051902.

35 W. B. Russel, D. A. Saville and W. R. Schowalter, *Colloidal Dispersions*, Cambridge University Press, Cambridge, 1st edn, 1992.
36 S. Thutupalli, R. Seemann and S. Herminghaus, *New J. Phys.*, 2011, **13**, 073021.
37 Y. Nakayama, K. Kim and R. Yamamoto, *Eur. Phys. J. E: Soft Matter Biol. Phys.*, 2008, **26**, 361–368.
38 T. Iwashita, Y. Nakayama and R. Yamamoto, *J. Phys. Soc. Jpn.*, 2008, **77**, 074007.
39 A. Hamid and R. Yamamoto, *J. Phys. Soc. Jpn.*, 2013, **82**, 024004.
40 K. Kim, Y. Nakayama and R. Yamamoto, *Phys. Rev. Lett.*, 2006, **96**, 208302.
41 H. Kobayashi and R. Yamamoto, *J. Chem. Phys.*, 2011, **134**, 064110.
42 R. Tatsumi and R. Yamamoto, *Phys. Rev. E: Stat., Nonlinear, Soft Matter Phys.*, 2012, **85**, 066704.
43 X. Luo, M. R. Maxey and G. E. Karniadakis, *J. Comput. Phys.*, 2009, **228**, 1750–1769.
44 S. Ramachandran, P. B. Sunil Kumar and I. Pagonabarraga, *Eur. Phys. J. E: Soft Matter Biol. Phys.*, 2006, **20**, 151–158.
45 M. T. Downton and H. Stark, *J. Phys.: Condens. Matter*, 2009, **21**, 204101.
46 I. Götze and G. Gompper, *Phys. Rev. E: Stat., Nonlinear, Soft Matter Phys.*, 2010, **82**, 041921.
47 J. F. Brady and G. Bossis, *Annu. Rev. Fluid Mech.*, 1988, **20**, 111–157.
48 J. W. Swan, J. F. Brady, R. S. Moore and ChE 174, *Phys. Fluids*, 2011, **23**, 071901.
49 T. Ishikawa and T. J. Pedley, *Phys. Rev. Lett.*, 2008, **100**, 088103.
50 J. V. José and E. J. Saletan, *Classical Dynamics: A Contemporary Approach*, Cambridge University Press, New York, 1st edn, 1998.
51 Y. Han, A. M. Alsayed, M. Nobili, J. Zhang, T. C. Lubensky and A. G. Yodh, *Science*, 2006, **314**, 626–630.
52 J.-P. Hansen and I. R. McDonald, *Theory of Simple Liquids*, Academic Press, New York, 3rd edn, 2008.
53 J. Padding and A. Louis, *Phys. Rev. Lett.*, 2004, **93**, 220601.
54 D. A. McQuarrie, *Statistical Mechanics*, University Science Books, Sausalito, 1st edn, 2000.
55 I. Llopis and I. Pagonabarraga, *J. Non-Newtonian Fluid Mech.*, 2010, **165**, 946–952.

